

SUPPLEMENTAL INFORMATION

PTEN C-terminal Deletion Causes Genomic Instability and Tumor Development

Zhuo Sun,^{1,2} Chuanxin Huang,² Jinxue He,² Kristy L. Lamb,² Xi Kang,^{1,2} Tingting Gu,² Wen Hong Shen,^{2,*} and Yuxin Yin^{1,2,*}

¹Institute of Systems Biomedicine, Peking University Health Science Center, Beijing, 100191, P.R. China

²Department of Radiation Oncology, Weill Medical College of Cornell University, New York, NY 10065, USA

*Correspondence: yinyuxin@hsc.pku.edu.cn or wes2007@med.cornell.edu

SUPPLEMENTAL INFORMATION

Supplemental Figures S1-S6
Supplemental Tables S1-S2

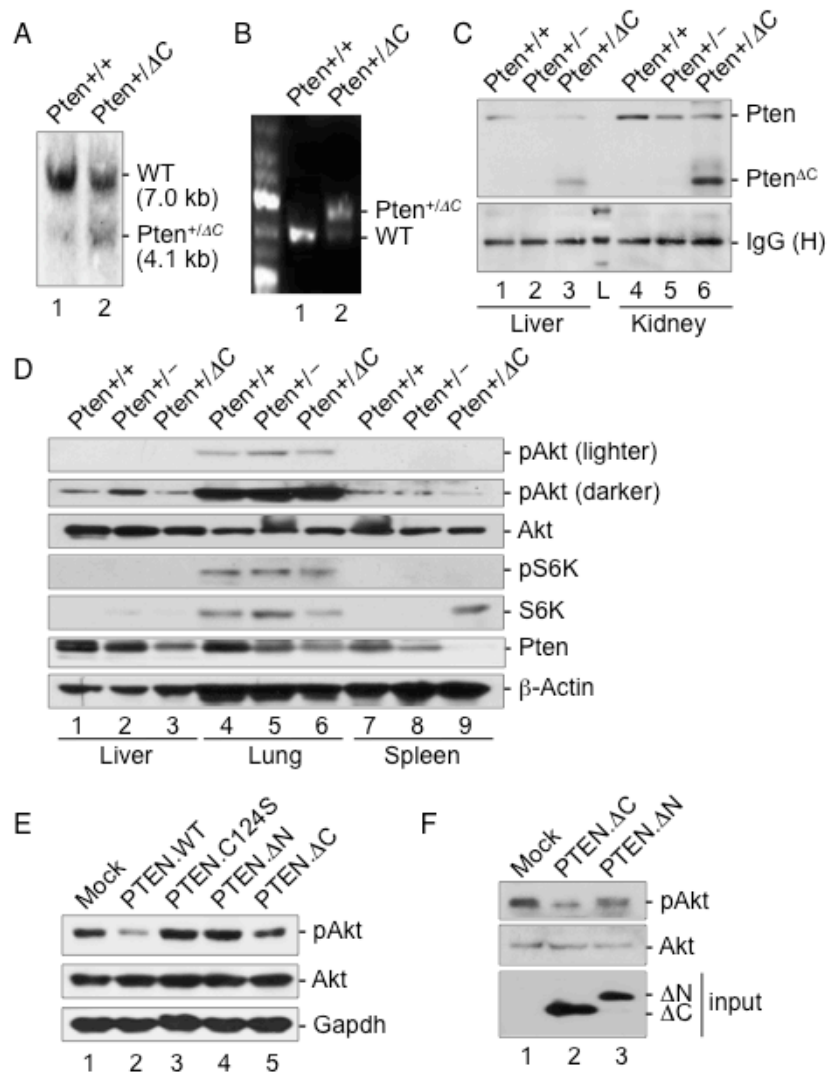


Figure S1, related to Figure 1. Verification of *Pten* truncation and evaluation of *Pten* ^{Δ C} phosphatase activity

(A) Southern blot analysis of wild-type and knock-in ES clones after digestion with *EcoRI* and *NcoI* and hybridization with the probe as indicated in Figure 1A. (B) Genotyping PCR analysis of tail DNA from *Pten*^{+/+} and *Pten*^{+/ Δ C} mice. (C) Expression of Pten (55 kDa) and Pten ^{Δ C} (~28 kDa) in *Pten*^{+/ Δ C} MEFs. Different tissues from *Pten*^{+/+}, *Pten*^{-/-} and *Pten*^{+/ Δ C} mice were subjected to immunoprecipitation with a N-terminal specific PTEN antibody (N-19, Santa Cruz) followed by immunoblotting with a homemade full-length PTEN antibody. L, protein ladder. (D) Various tissues from *Pten*^{+/+}, *Pten*^{-/-} and *Pten*^{+/ Δ C} mice were lysed for Western analysis of downstream effectors of PI3K activity including phosphorylated Akt and S6K. (E) Akt expression levels and phosphorylation were analyzed in *Pten*^{-/-} MEFs transfected with wild-type PTEN and different PTEN mutants. PTEN.C124S, a phosphatase-deficient mutant; PTEN. Δ C, PTEN C-terminal truncated mutant; PTEN. Δ N, a mutant lacking the N-terminus. (F) *In vitro* dephosphorylation assay. His-tagged PTEN fragments (Δ C and Δ N) were purified with Ni-NTA beads and incubated with protein lysates from *Pten*^{-/-} MEFs. Phosphorylation of Akt and its total levels were evaluated by Western analysis.

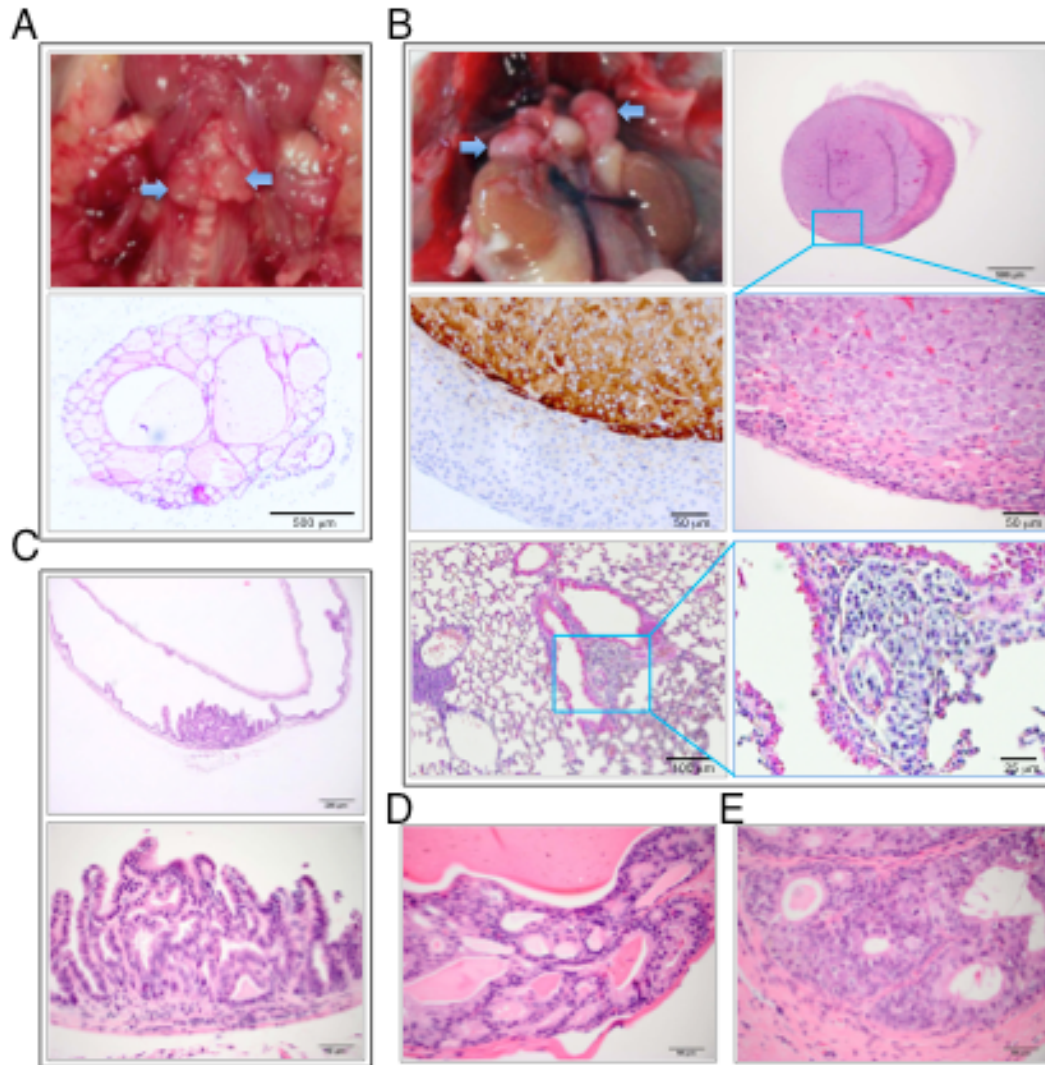


Figure S2, related to Figure 2. Additional neoplastic lesions in multiple tissues of *Pten*^{+/-AC} mice

(A) Bilateral thyroid goiter (blue arrows). (B) Adrenal pheochromocytoma. Top-left, enlarged adrenal glands (bilateral, blue arrows); Top-right and mid-right, pheochromocytoma showing marked expansion of the adrenal medulla by a demarcated neoplasm that severely compresses adjacent adrenal cortex; Mid-left, cytoplasmic expression of chromogranin in pheochromocytoma cells; bottom images, pulmonary pheochromocytoma metastasis in the alveolar wall, showing a cluster of cells that cytologically resemble the neoplastic cells in the primary adrenal medulla. (C) Polypoid adenoma of the gallbladder mucosa showing a sessile proliferative lesion consisting of papillary projections of plump epithelial cells. (D) Prostatic intraepithelial neoplasia (PIN) showing proliferation of epithelium with cribriform architecture. (E) Epididymitis showing marked luminal dilation and thickened epithelium due to disorganized proliferation of epithelial cells.

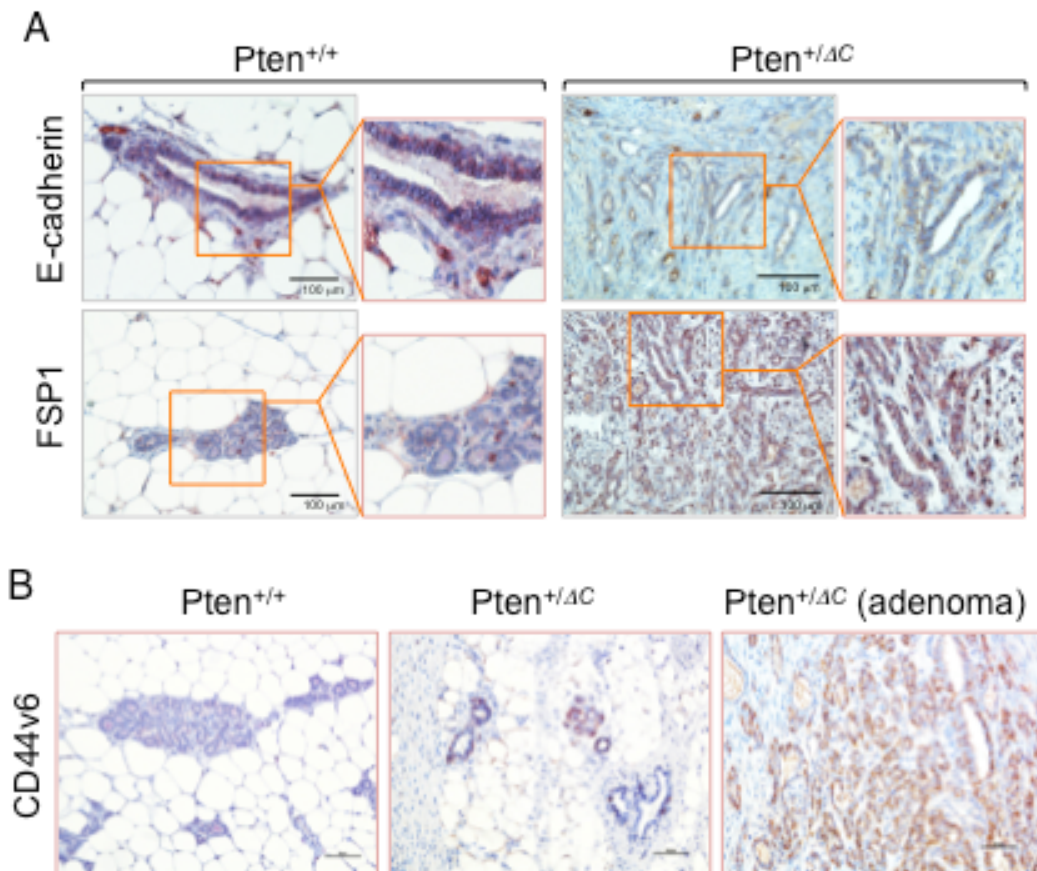


Figure S3, related to Figure 2. Occurrence of EMT in *Pten*^{+/ Δ C} mammary adenoma
(A) Two EMT markers, E-cadherin and FSP-1 (fibroblast specific protein-1), were analyzed with immunohistochemistry in mammary adenomas in *Pten*^{+/ Δ C} mice using *Pten*^{+/+} normal mouse breast tissues as a control. As expected in EMT, E-cadherin expression is decreased and FSP-1 is increased in breast adenoma from *Pten*^{+/ Δ C} mice.
(B) Immunohistochemistry staining of a CD44 variant, CD44v6, in breast tissues from *Pten*^{+/+} and *Pten*^{+/ Δ C} mice. Breast adenoma from *Pten*^{+/ Δ C} mice shows an increased level of CD44v6.

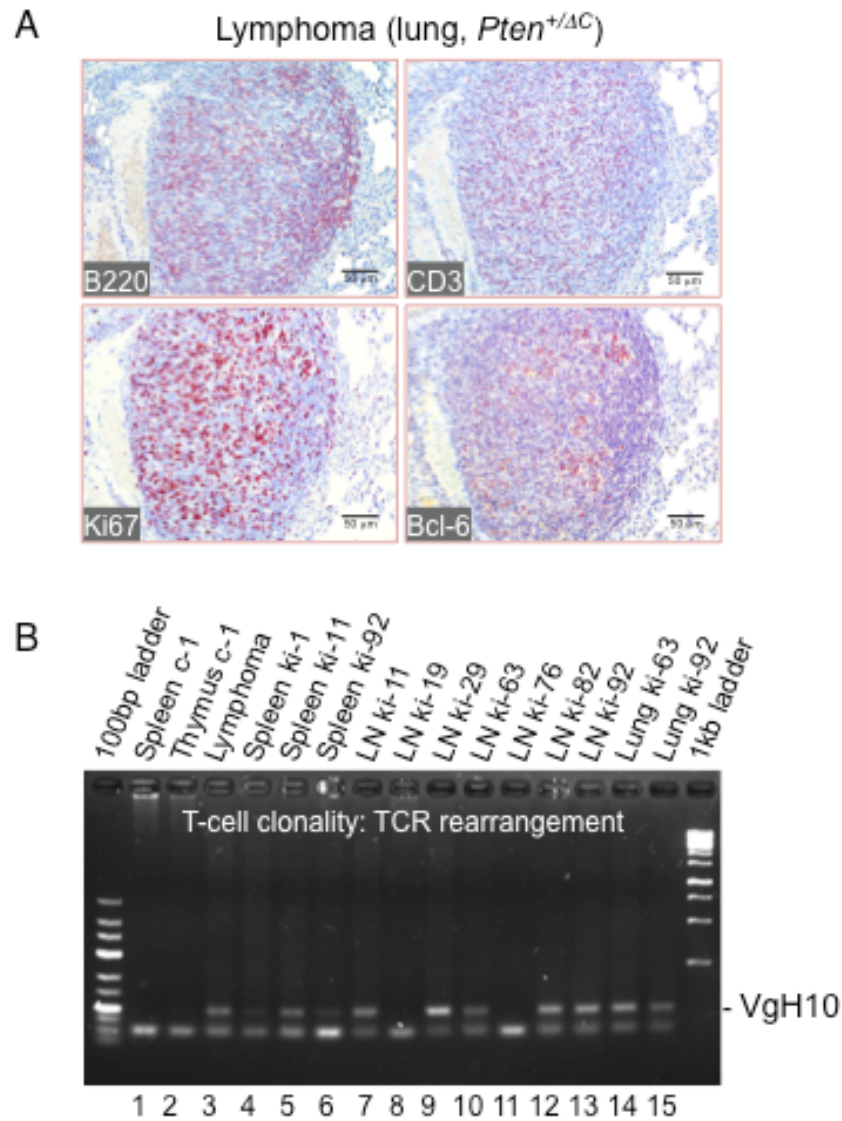


Figure S4, related to Figure 3. *Pten*^{+ΔC} mice exhibit lymphomatous infiltrations of proliferative B and T cells in the lung

(A) Lung tissues from *Pten*^{+ΔC} mice with lymphocytic infiltration were stained for B and T cell, cell proliferation markers and Bcl-6 as indicated by immunohistochemistry. (B) Clonality analysis showing clonal T cell receptor g chain rearrangement (for T-cell lineage) in most biopsies from *Pten*^{+ΔC} mice (lanes 3-7, 9, 10, 12-15) as indicated.

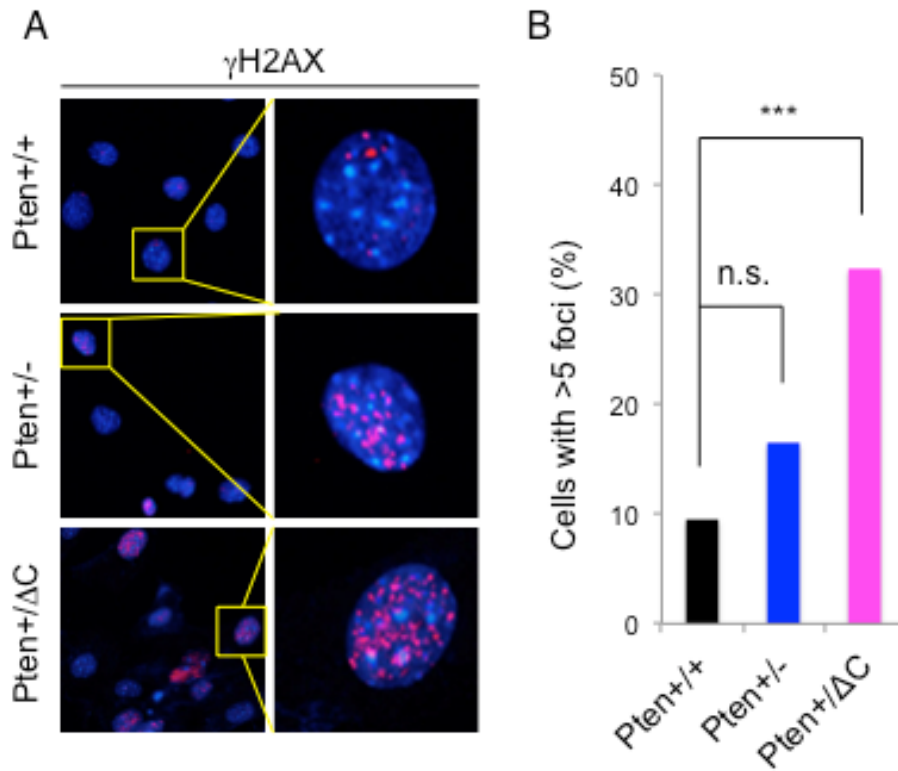


Figure S5, related to Figure 4. PTEN C-terminal deficiency promotes double strand DNA breaks

Immunofluorescence analysis of γ H2AX in *Pten*^{+/+}, *Pten*^{+/-} and *Pten*^{+/- Δ C} MEFs (**A**) and a summary of cells with >5 γ H2AX foci (**B**). n.s., not significant; ***, $p < 0.001$.

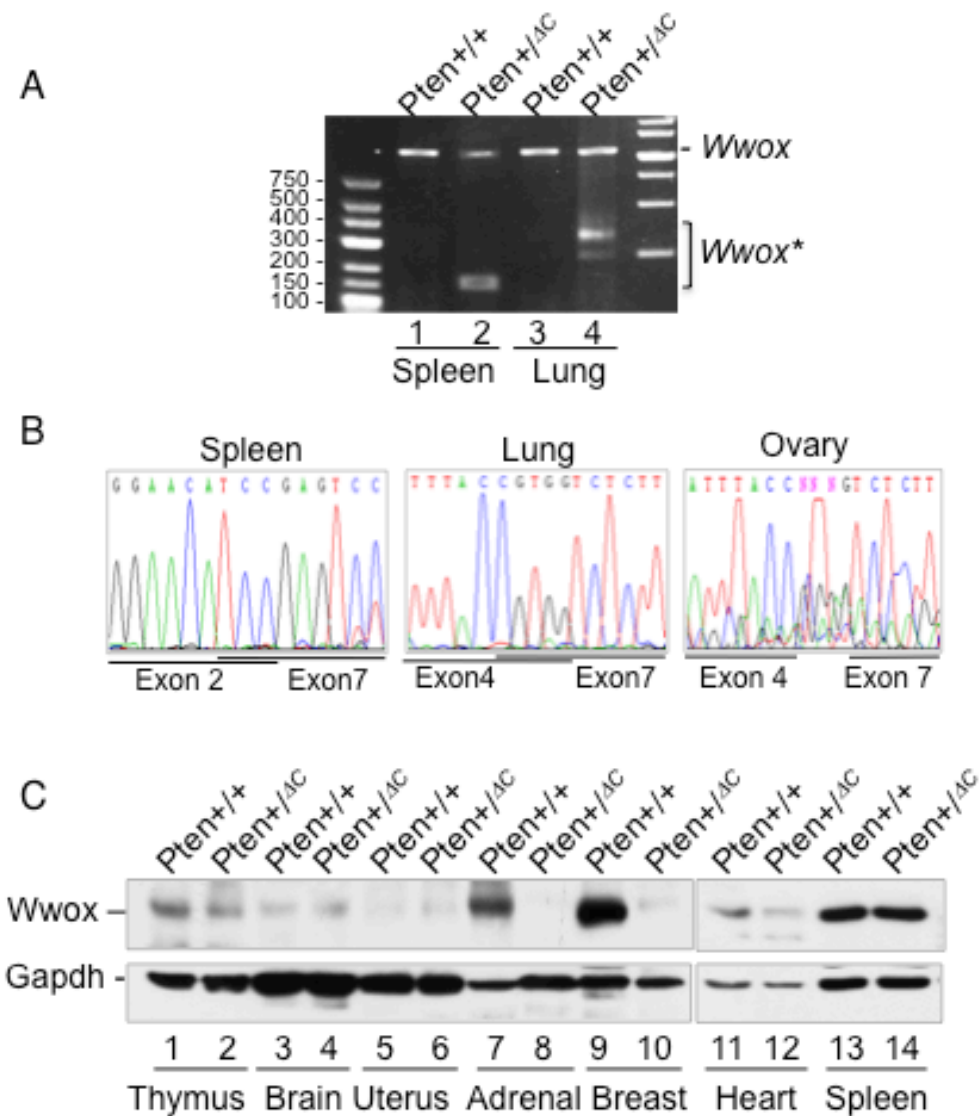


Figure S6, related to Figure 5. Knock-in of *Pten*^{ΔC} causes common fragile site rearrangement

(A and B) Abnormal transcripts of the *Wwox* gene in *Pten*^{+/-ΔC} tissues due to alternative splicing and rearrangement. (C) Reduced expression of *Wwox* in *Pten*^{+/-ΔC} tissues as indicated as compared with those from *Pten*^{+/+} mice.